Current Biology 19, 398–403, March 10, 2009 ©2009 Elsevier Ltd All rights reserved DOI 10.1016/j.cub.2009.01.037

Report

Functional MRI Evidence for LTP-Induced Neural Network Reorganization

Santiago Canals,[1,4,*] Michael Beyerlein,[1] Hellmut Merkle,[3] and Nikos K. Logothetis[1,2]

[1]Max Planck Institute for Biological Cybernetics
72076 Tübingen
Germany

[2]Imaging Science and Biomedical Engineering
University of Manchester
Manchester M13 9PL
UK

[3]National Institute of Neurological Disorders and Stroke
Laboratory of Functional and Molecular Imaging
National Institutes of Health
Bethesda, MD 20892
USA

Summary

The hippocampal formation is a region of the forebrain that is important for memory and spatial navigation [1, 2]. On the basis of a vast amount of literature, the hippocampus is linked with long-term potentiation (LTP), the increased synaptic strength following repeated stimulation of the hippocampal neurons [3, 4]. LTP is considered to be the experimental demonstration of Hebb's postulate on synaptic strength and learning [5], and it is the dominant model of an experience-dependent modification of brain circuits. Yet, despite the importance of this phenomenon for brain physiology and behavior, little is known about how experimentally measured regional synaptic modifications alter the activity of global, widespread networks. Here, we use simultaneous fMRI, microstimulation, and electrophysiology [6–8] to unveil global changes in brain activity due to local hippocampal plasticity. Our findings offer the first evidence of an LTP-induced network reorganization that includes increased interhemispheric communication and recruitment of limbic and neocortical circuits after changes in synaptic strength within the hippocampus.

Results and Discussion

We scanned 14 urethane-anesthetized rats in a 4.7 T magnet while stimulating the main cortical input of the hippocampal formation, the perforant path. In previous experiments, we had demonstrated that electric pulses delivered to the perforant path sequentially activate all the structures of the hippocampal formation (DG, CA3, CA1, and subiculum and entorhinal cortex) in an intensity- and frequency-dependent manner [8]. The maps obtained in those experiments were highly reproducible across animals and experimental protocols.

In the present study, we examine possible changes in the BOLD signal and concomitant activation maps that follow regional (i.e., LTP of the perforant path) as well as potential global modifications of synaptic strength. More specifically, we recorded neural and fMRI signals before and after the induction of LTP with a protocol of high-frequency stimulation (HFS) of the perforant path (for details, see Experimental Procedures). Figure 1 shows the robust potentiation of neural responses (LTP_{Phys}) that is reflected in both the slope of the population excitatory postsynaptic potentials (EPSPs) and the amplitude of the population spikes (PSs) (Figure 1A, left panel) and in the fMRI BOLD (LTP_{BOLD}) signal (Figure 1A, right panel) originating from mass activation [9]. The lower panels of Figure 1A show the location of the electrodes and the activation induced by stimulation. One hour after the HFS, the EPSP slope and the PS and BOLD amplitudes in the DG increased (Figures 1B and 1C; 128% ± 9%, 228% ± 33%, and 124% ± 8%, respectively, mean ± SEM, n = 6 animals). This increase was found to last for at least 3 hr and repeatedly exhibited very similar time courses (Figure 1D). With this particular HFS protocol, LTP induction was highly effective (<10% of HFS failed to induce LTP; these data were not included in the group analysis), and LTP_{Phys} was always accompanied by a concomitant LTP_{BOLD}. Further investigations will be designed to compare the results obtained with different HFS protocols. To further investigate the time course and dynamics of LTP_{BOLD}, we continuously recorded the electrical and BOLD signals before, during, and after the induction phase. The latter protocol permits an assessment of the stability of the BOLD baseline and the elimination of confounding factors originating in fluctuations in the MR signal itself. Figure 1E shows the effects of stimulation on both neural and BOLD signals over a long period of over 20 min. Signal modulation is clearly enhanced after LTP induction without any substantial changes in baseline activity. This result was expected after our control experiments examining the temporal stability of the signals over long periods such as those required for the demonstration of the LTP effects. Both electrophysiological and hemodynamic signals showed a stable baseline and modulation during the blocks of stimulation used to generate fMRI maps (4–8 min) and over the complete experimental session (3–4 hr, Figure S1 available online). Moreover, current intensity, PSs, and the slope of the EPSPs were all linearly correlated with the amplitude of the BOLD signal in the DG around the recording electrode tip (Figure 2). The latter result is in good agreement with previously reported data in awake and anesthetized monkey [7, 10].

Finally, we tested the NMDA channel dependency of the LTP_{BOLD}. It is well known that the induction of LTP_{Phys} in the DG is prevented by NMDA channel antagonists [11, 12]. Administration of 0.5 mg/kg (i.p.) of the noncompetitive inhibitor MK-801 moderately decreased the LFP and fMRI signal amplitude (Figures 3A and 3B). When applied 30 min before the HFS of the perforant path, MK-801 totally abolished the induction of both LTP_{Phys} and LTP_{BOLD} (Figures 3B–3D, n = 4). All in all, the relative magnitude, temporal evolution, and pharmacology of the fMRI responses strongly indicate that LTP_{BOLD} reflects the classical LTP of synapses in the hippocampus. These results therefore represent the first unambiguous demonstration of synaptic plasticity by means of fMRI.

*Correspondence: scanals@iib.uam.es

[4]Present address: Instituto de Neurociencias CSIC-UMH, Campus de San Juan, 03550 San Juan de Alicante, Spain

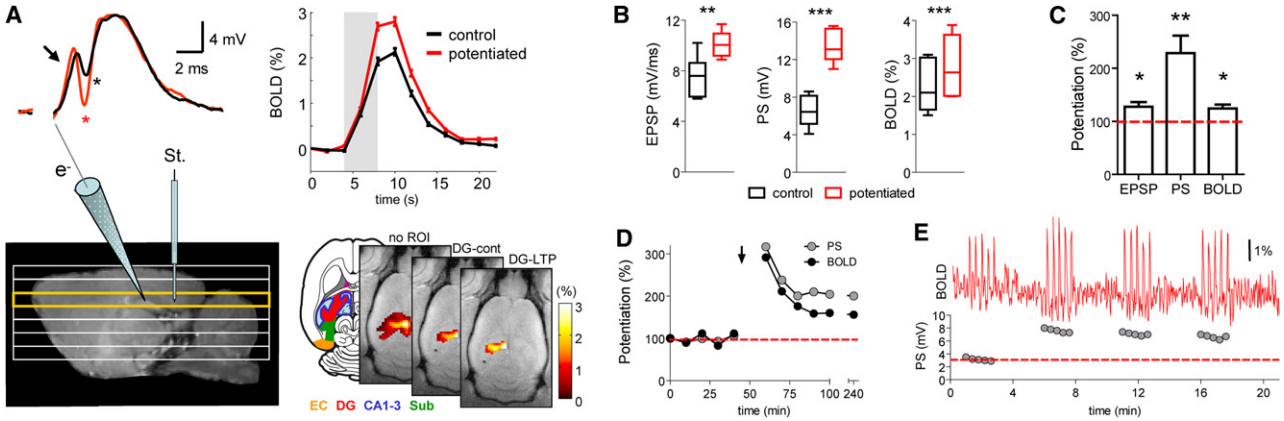

Figure 1. Long-Term Potentiation of Electrophysiology and fMRI Signals

(A) The left upper panel shows changes in the local field potential (LFP), specifically the population excitatory postsynaptic potential (EPSP) and the population spike (PS), and the right upper panel shows the time course of BOLD signal (mean ± SEM) in the DG of one animal before (black) and 1 hr after (red) high-frequency stimulation (HFS) of the perforant path. The arrow points to the EPSP, and asterisks mark the peak of the PS. The relative position of EPI slices (bottom right) and the stimulation (St.) and recording (e^-) electrodes are indicated on a sagittal, high-resolution anatomical scan (lower-left panel). The BOLD signal was analyzed in a region of interest (ROI) containing the area of DG around the recording electrode (lower-right panel). The thresholded ($p < 0.01$) functional maps, here overlaid on FLASH anatomical scans, show the activation in the hippocampus (no ROI) and the DG before (DG-contr) and after (DG-LTP) HFS. The left-most drawing, modified from the Paxinos and Watson rat brain atlas [27], delineates the regions of interest: EC, entorhinal cortex; Sub, subiculum. The slice containing the DG-ROI is marked in yellow on the left panel.

(B and C) Group analysis showing the simultaneous potentiation of electrophysiology and fMRI signals (n = 6). Data in (B) are plotted as box and whiskers (with whiskers as min. and max. values) and in (C) as mean ± SEM.

(D) Time course of LTP_{PHYS} and LTP_{BOLD} in a representative animal. The figure shows the evolutions of the augmentations of PSs and active brain volume up to 3 hr after HFS (arrow).

(E) Dynamics of BOLD signal and PS amplitude over the course of an LTP protocol.

An obvious question raised by these findings is the extent to which changes in local synaptic plasticity affect global activation patterns of networks, including the site of LTP induction. Indeed, we found that LTP_{BOLD} is characterized not only by a local hippocampal increase in signal amplitude that is comparable to classical electrophysiological findings [3, 4, 11, 12] but also by a spread of activity across and beyond the hippocampus (Figures 4A and 4B). More specifically, after HFS, the activation of the perforant path affected large areas of the hippocampal formation, including the hippocampus proper, the subiculum and the entorhinal cortex (Figures 4A–4C). Interestingly, hippocampal and entorhinal recruitment was prominent in the contralateral hemisphere (Figure 4D). In fact, the relative potentiation was significantly higher in the contralateral formation (Figure 4E, 159% ± 25% and 379% ± 52% for ipsi- and contralateral activation, respectively, $p = 0.006$). Together with a previous report on bilateral hippocampal neurotrophin and trk receptor mRNA expression as a consequence of unilateral LTP [13], our data argue for a potentiated interhemispheric communication based on unilateral strengthening of synaptic weights. Of greatest interest, however, was the significant activation that we found outside of the hippocampal formation in four out of six LTP experiments, namely in the perirhinal cortex (PRh), the prefrontal cortex (PFC), the nucleus accumbens (Acb), and the anterior olfactory nucleus (AON). These activations were entirely contingent on LTP induction (Figure 4A). In controls in which the perforant path was stimulated with high current intensities before HFS, thus saturating the amplitude of the PS (up to 1.0 mA), we never observed activation in any of the aforementioned extrahippocampal structures (data not shown, see [8]). The recruitment of brain areas after LTP was

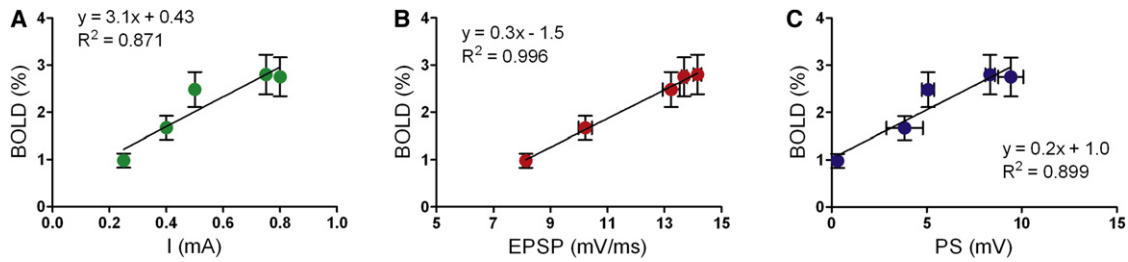

Figure 2. Correlation of BOLD and Electrophysiological Signals

The increment in BOLD signal (%) in the dentate gyrus during perforant path stimulation is plotted against the current intensity used for stimulation (A), the recorded excitatory postsynaptic potential (EPSP) in the dentate gyrus (B), and the corresponding population spike (PS) (C). BOLD, EPSP, and PS represent the mean ± SEM of all hemodynamic, synaptic, and spiking responses, respectively, during a complete experiment (n = 5 experiments, collected in four different animals). Data are fitted with linear regression.

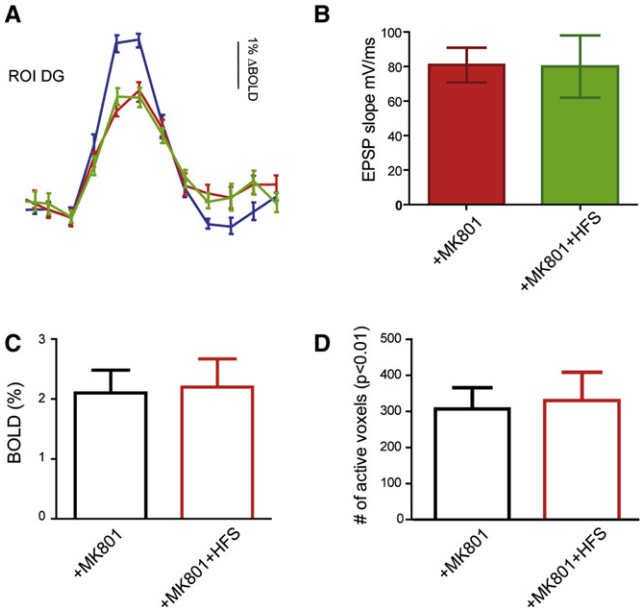

Figure 3. The NMDA Receptor Antagonist MK-801 Prevents the Induction of Both LTP_{phys} and LTP_{BOLD}

The mean BOLD time courses in the dentate gyrus (DG) of a representative experiment (A) and the slope of the EPSP in the DG normalized to the control values (B) of n = 3 experiments are shown before and 30 min after an i.p. injection of MK-801 (5 mg/Kg) (blue and red labeling, respectively). A reduction in the fMRI and electrophysiological signals was observed after MK-801 treatment. The failure to induce LTP_{phys} and LTP_{BOLD} after a protocol of high-frequency stimulation in the presence of the NMDA antagonist was demonstrated and is shown by green labeling in (A) and (B). (C) shows the group analysis (n = 4) corresponding to panel (A). (D) shows recruitment of new brain structures after LTP is prevented by administration of MK-801 30 min before HFS (n = 4). Error bars in all panels represent SEM.

also prevented by MK-801 (Figure 3D), demonstrating a shared NMDA receptor dependency of both synaptic and network plasticity and suggesting a causal relationship.

On the basis of the terminal fields of the perforant path projection [14] and the known physiological responses to high-frequency microstimulation in the hippocampus, the site of LTP induction that triggers the above-described network reorganization must be located in the subfields of the ipsilateral hippocampal formation. Perforant path synapses susceptible to LTP have been described mainly in the DG, but also in CA3 and CA1 [15, 16]. Direct activation of remote—polysynaptic—extrahippocampal structures and therefore potential participation of such structures in network plasticity are unlikely given that the HFS protocol was delivered at 200 Hz, and perforant path stimulation at high frequencies (>20 Hz) is known not to propagate polysynaptically [8, 17]. On the other hand, stimulation frequencies lower than 20 Hz (similar to what we use as test stimulus) greatly enhance polysynaptic excitation of pyramidal neurons [8, 17]. Thus, the polysynaptic activation of brain areas after LTP, both in the contralateral hippocampus and extrahippocampal structures, is most probably the result of potentiated synaptic currents elicited by a test stimulus delivered at a frequency able to spread multisynaptically.

We can not categorically rule out a possible contribution of the crossed perforant path projection to the contralateral hippocampal activation. However, the very reduced number of these fibers compared to the ipsilateral projection [14] and the finding that monosynaptic activation of the perforant path (at high frequency) did not elicited BOLD responses in the contralateral hippocampus while producing a complete and strong activation in the ipsilateral [8] strongly suggest that the LTP-triggered increase in contralateral activation actually represents increased commissural-associational communication. Although further experimentation will be required to unveil its functional meaning, we speculate that this potentiated commissural communication could be relevant for pattern completion in the rat. The CA3 network is thought to operate as an autoassociative memory with capability to selectively retrieve a specific pattern of firing activity (from among several possible patterns) when provided with a partial environmental cue (for a review, see [18]). This property relies on the associational connections of CA3, which largely represents the most prominent input to this hippocampal subfield [14], and on the presence of NMDA channels on them [19]. In the rat, CA3 pyramidal cells establish associational connections with the ipsilateral CA3 (recurrent collaterals), and also with the contralateral CA3, CA2, and CA1 (commissural projection) [14]. In this way, the NMDA-dependent recruitment of contralateral hippocampal regions reported here may represent one feature of the pattern-completion mechanism. In the presence of partial cues in the environment, ipsilateral potentiation of synaptic inputs could promote cooperative bilateral reconstruction of incomplete memory traces and thus improve pattern-completion and memory recall or consolidation. In rats, with their largely crossed visual systems, the presence of a high degree of plastic and dynamic interhippocampal communication may also have been advantageous to coherently build cognitive maps from visually evoked place cells. In animals with reduced (or absent) associational connections such as primates [14], which present more lateralized distribution of functions between both hippocampus, pattern completion would be accomplished unilaterally.

Functional connections of the AON, PFC, PRh, and Acb with the hippocampal formation are well supported by the neuroanatomical data. All these structures receive strong projections from the hippocampal formation and send back projections to it [14]. Moreover, links between these structures have been established in the context of LTP, learning, and memory. For instance, the administration of the NMDA channel blocker AP5 to animals after they had been trained in odor discrimination impaired new learning without affecting retention [20]. Entorhinal lesions cause rapid forgetting of olfactory information [21]. Therefore, the recruitment of AON, as well as that of the other activated structures observed in our experiments, is in good agreement with previous results on the connectivity of hippocampal formation and its putative function.

In conclusion, by combining fMRI with the well-established LTP protocol, we demonstrated long-lasting changes in the activity of the entire brain, most likely triggered by local modifications in synaptic transmission. In particular, our observations unveil new features of the hippocampal LTP, demonstrating that the local strengthening of synaptic weights modulates the brain's functional connectivity—network plasticity—in a way that (1) potentiates the bilateral communication of the hippocampal formation and (2) effectively recruits specific cortical and subcortical structures. It is interesting to note that, on the basis of neuroanatomical knowledge (for a recent review, see [14]), the number of targets of the hippocampal output greatly exceeds the number of extrahippocampal structures shown in our LTP_{BOLD} maps, suggesting that the

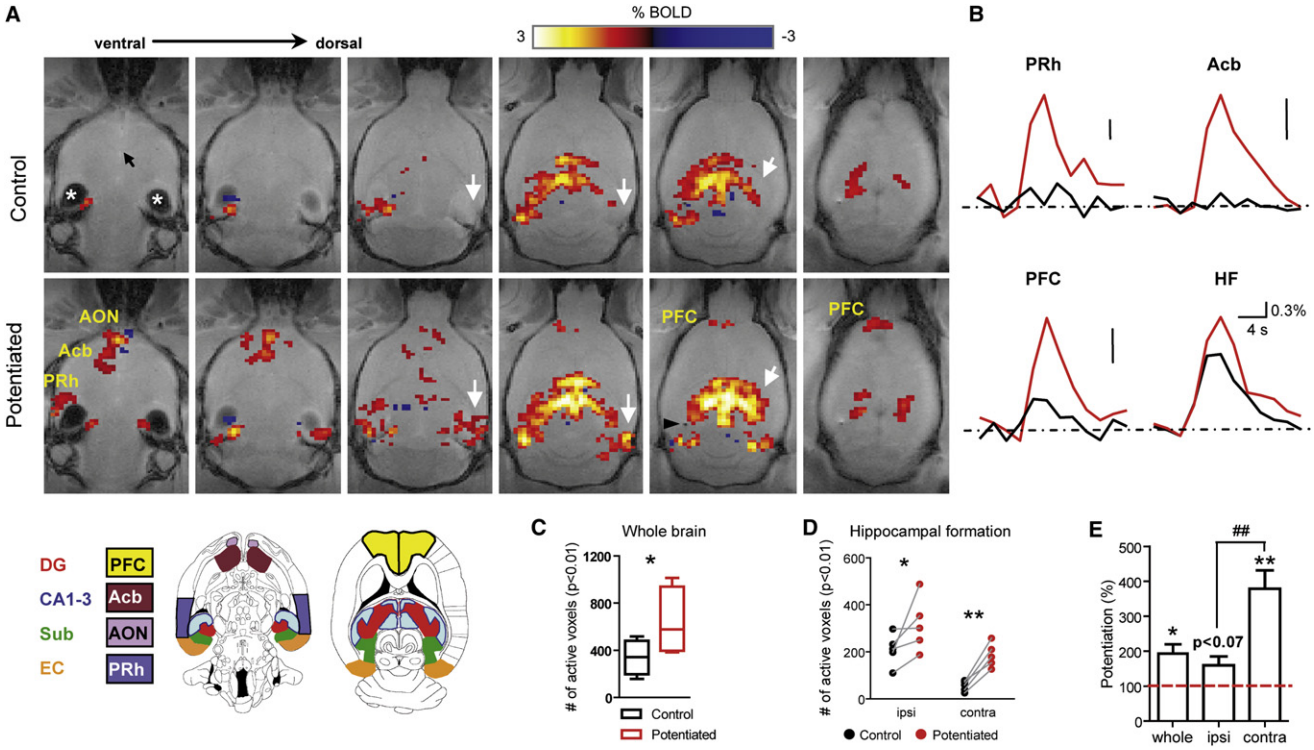

Figure 4. Long-Lasting Changes in Network Organization after Hippocampal LTP

(A) Functional maps thresholded and overlaid on horizontal FLASH anatomical scans, showing brain active areas during perforant path stimulation before (control) and after HFS (potentiated). New structures recruited after LTP of hippocampal synapses include the nucleus accumbens (Acb), the anterior olfactory nucleus (AON), and the perirhinal (PRh) and prefrontal cortex (PFC). White arrows point to corresponding brain areas contralateral to the stimulated perforant path. The black arrow points to the anterior commisure, and asterisks mark image artifacts due to the ear channel. The color-coded scale represents positive and negative BOLD response in percent change from baseline. The position of the tip of the stimulation electrode is marked by the black arrowhead. The inset drawings, modified from the Paxinos and Watson rat brain atlas [27], delineates different regions of interest.

(B) BOLD signal time courses at the indicated ROIs before (black) and after (red) HFS (HF, hippocampal formation).

(C) Number of significantly ($p < 0.01$) active voxels (volume of activated brain) before (black) and after (red) HFS (box and whiskers plot as in Figure 1, n = 5). *$p < 0.05$, paired t test.

(D) Group data showing number of active voxels in the hippocampal formation ipsi- and contralateral to the stimulated perforant path (n = 5). *$p < 0.05$, **$p < 0.01$, unpaired t test before versus after HFS.

(E) Relative potentiation of the recruitment of active tissue in the complete brain (whole) and the hippocampus, again ipsilateral (ipsi) and contralateral to the stimulated perforant path (mean ± SEM). *$p < 0.05$, **$p < 0.01$, unpaired t-test before versus after HFS, and $^{\#\#}p < 0.01$, unpaired t test ipsi versus contra.

functional consequences of synaptic potentiation do not uniformly affect the entire anatomically defined network. This might be due in part to differences in the connectivity of various groups of entorhino-hippocampal neurons, which differentially distribute the effects of modification in their synaptic weights. The nature of the recruited structures found in this study indicates an increased communication between higher-order associational and polysensory cortices with the cortical and subcortical limbic network subserving memory [1, 2, 14, 22–24]. These results are consistent with information channeling or operational segregation within the hippocampal formation. Future work will be directed toward an electrophysiological understanding of the information flow in the LTP-opened channels in the context of memory formation, consolidation, and retrieval.

Experimental Procedures

A total of 14 male Sprague-Dawley rats (250–300 g) were used in the present study. All experiments were approved by the local authorities (Regierungspraesidium) and were in full compliance with the guidelines of the European Community (EUVD 86/609/EEC) for the care and use of the laboratory animals.

Electrode Implantation, Microstimulation, and Recordings

The animals were anesthetized with urethane (1.2–1.5 g/kg, i.p.). There is considerable experience with this anesthetic in in vivo rat electrophysiological experiments in general and in LTP experiments in particular. In a previous report, we demonstrated that it is also a good anesthesia for fMRI experiments with BOLD contrast [8]. In addition, LTP experiments in awake and freely moving rats suggest that the main concepts about LTP are consistent across animal preparations including awake and anesthetized in vivo experiments, as well as in vitro slice preparations.

Standard surgical and stereotaxic procedures were applied for the placement of recording and stimulating electrodes, as previously described [8, 25, 26]. A glass-coated iridium (100 μm diameter, 50–80 kΩ) monopolar electrode was positioned in the medial perforant path (from lambda: 0 mm anteroposterior and 4.1–4.5 mm lateral, 2.5–3 mm ventral to the dural surface) for orthodromic stimulation of the dentate gyrus (DG) and the hippocampus proper [27]. Recording electrodes were glass micropipettes filled with isotonic NaCl (1–1.5 MΩ) and placed at the hilus of the DG (3.5 mm caudal and 2.5 mm lateral from bregma) guided by the typical evoked potentials [28]. A subcutaneous Ag/AgCl wire electrode under the skin of the neck was used as a reference and ground. The final placement of the stimulating and recording electrodes was adjusted so that a maximum population spike (PS) in the DG was induced. Both electrodes were secured to the skull with dental cement and plastic screws, and the animal moved to the scanner and was fixed in a custom-made MRI-compatible stereotaxic device (see below). The position of the stimulating electrode was further confirmed by means of anatomical scans.

In the scanner, the recording and stimulating electrodes were connected to a custom-built amplifier and constant current source, respectively [6, 8]. The exposed skull was covered with agar to minimize magnetic susceptibility artifacts at air-tissue interfaces. The current amplitude, pulse duration, train duration, and stimulation frequency were controlled digitally with custom-made software running on the QNX (Canada) real-time operating system. The stimulation protocol was a block design consisting of 10 or 20 periods of 4 s stimulation epochs followed by resting epochs of 20 s (4 or 8 min in total, respectively). This protocol was repeated three to five times per animal and condition. The stimulation pulses were always biphasic and charge balanced, with the cathodal pulse leading the anodal pulse and a pulse duration of 0.2 ms. The capacitance of the cable connecting the stimulating electrode to the current source was compensated to allow the delivery of fast (hundreds of microseconds) and quasisquare electric pulses to the tissue [6].

Before beginning with MRI data collection, we generated standard input-output curves of the DG by plotting the amplitude of the PS in the evoked field potential induced by single shocks to the perforant path against the intensity of the applied current (0.1–1 mA). For the MRI experiments, the current required to induce a PS of 50% maximal amplitude was applied during the stimulation periods (483 ± 49 μA, mean ± SEM of all experiments). The 4 s stimulation (test stimulus) consisted of pairs of pulses with 100 ms interpulse intervals that were repeated after 300 ms (3.3 Hz). This protocol did not induce long-lasting synaptic plasticity by itself (see Figure S1). LTP was induced by high-frequency stimulation of the perforant path with episodes of six trains of pulses (each train delivered at 200 Hz and lasting 40 ms, with four pulses per train and trains delivered every 10 s) repeated three times with pauses of 2 min between episodes (modified from [29]) (see Figure S2). In some experiments devoted to following LTP induction, test stimuli were intermingled with high-frequency trains.

After filtering (0.3 Hz–3 kHz) and amplification, the electrophysiological signals were digitalized (22.3 kHz acquisition rate) and stored in a personal computer for offline processing with MatLab and Spike2. MRI-derived artifacts were removed from the signal with our own code written in MatLab, as described previously [7, 30]. The PS in the hilus of the DG was measured as the amplitude from the precedent positive crest, and the negative peak and the excitatory postsynaptic potential (EPSP) were measured as the maximal slope of the rising potential preceding the PS.

MR Imaging

For the MRI experiments, the urethane-anesthetized animals were placed in a custom-made saddle coil integrated within an animal and head holder (RAPID Biomedical, Rimpar, Germany) and modified to optimize the SNR. Temperature, heart rate, SpO_2, and breathing were monitored throughout the scanning session.

Experiments were carried out in a vertical 4.7 Tesla scanner with a 40 cm diameter bore (Biospec 47/40v, Bruker Medical, Ettlingen, Germany). The system had a 50 mT/m (180 ms rise time) actively shielded gradient coil (Bruker, BGA 26) of 26 cm inner diameter. Functional MRI was performed in seven axial slices with a GE-EPI sequence with the following parameters: FOV 48 mm (readout) × 32 mm (phase encoding), slice thickness 1 mm, matrix 96 × 64, four segments, FA 35°, TE 15 ms, and TR 500 ms. We used two types of anatomical scans to overlay the functional data and identify the activated brain areas. T-2-weighted anatomical images were collected with a rapid-acquisition relaxation-enhanced sequence (RARE), and the following parameters were applied: FOV 48 × 38 mm, seven slices, slice thickness 1 mm, matrix 240 × 160, TE_{eff} 80 ms, TR 5 s; a RARE factor of 8. T-1-weighted anatomical images were collected with the low-angle shot (FLASH) method with the following parameters: FOV 48 × 38 mm, seven slices, slice thickness 1 mm, matrix 256 × 128, FA 30°, TE 7 ms, and a TR of 750 ms. Additional FLASH images were acquired in the sagittal plane, with the image parallel to the electrode for visualization of the location of the electrode tip in the angular bundle (perforant path). The saddle coil, which was designed to generate a homogeneous field over the whole cortex and the hippocampus, was used for transmittal and receipt. The MR system is controlled by a Bruker BioSpec console (ParaVision 3) running under the Linux operating system.

Functional MRI data were analyzed offline with our own software developed in MATLAB and including the statistical parametric mapping packages (SPM2, www.fil.ion.ucl.ac.uk/spm). After linear detrending, temporal filtering (0.015–0.2 Hz) and spatial filtering (3 × 3 Gaussian kernel of 1.5 sigma) of voxel time series, general linear model or crosscorrelation analysis were applied with a simple boxcar model typically shifted forward in time by 2 s or with a boxcar convolved with a gamma probability-density function (MatLab) to account for the hemodynamic delay in the BOLD signal. Functional maps were generated from voxels that had a significant component for the model ($p < 0.01$, uncorrected) and were clustered together in space (connections in 18 neighboring directions with a minimum of 15 voxels).

Supplemental Data

Supplemental Data include two figures and can be found with this article online at http://www.current-biology.com/supplemental/S0960-9822(09)00609-5.

Acknowledgments

The authors acknowledge Yusuke Murayama for his help with data analysis and A. Oeltermann and M. Augath for technical support. This work was funded by a Long Term Fellowship from the Human Frontier Science Program, the Max Planck Society, and in part (H.M.) by the Intramural Research Program of the NIH (National Institute Neurological Disorders and Stroke), Bethesda, Maryland.

Received: December 5, 2008
Revised: January 12, 2009
Accepted: January 13, 2009
Published online: February 19, 2009

References

1. Scoville, W.B., and Milner, B.J. (1957). Loss of recent memory after bilateral hippocampal lesions. Neurol. Neurosurg. Psychiatry *20*, 11–21.
2. Squire, L.R., Stark, C.E.L., and Clark, R.E. (2004). The medial temporal lobe. Annu. Rev. Neurosci. *27*, 279–306.
3. Bliss, T.V.P., and Lømo, T.J. (1973). Long-lasting potentiation of synaptic transmission in the dentate area of the anaesthetized rabbit following stimulation of the perforant path. Physiol. (Lond.) *232*, 331–356.
4. Bliss, T.V.P., Collingridge, G.L., and Morris, R. (2007). Synaptic plasticity in the hippocampus. In The Hippocampus Book, P. Andersen, R. Morris, D. Amaral, T. Bliss, and J. O'Keefe, eds. (Oxford: Oxford University Press), pp. 343–474.
5. Hebb, D.O. (1949). The Organization of Behavior (New York: Wiley).
6. Tolias, A.S., Sultan, F., Augath, M., Oeltermann, A., Tehovnik, E.J., Schiller, P.H., and Logothetis, N.K. (2005). Mapping cortical activity elicited with electrical microstimulation using FMRI in the macaque. Neuron *48*, 901–911.
7. Logothetis, N.K., Pauls, J., Augath, M., Trinath, T., and Oeltermann, A. (2001). Neurophysiological investigation of the basis of the fMRI signal. Nature *412*, 150–157.
8. Canals, S., Beyerlein, M., Murayama, Y., and Logothetis, N.K. (2008). Electric stimulation fMRI of the perforant pathway to the rat hippocampus. Magn. Reson. Imaging *26*, 978–986.
9. Logothetis, N.K. (2008). What we can do and what we cannot do with fMRI. Nature *453*, 869–878.
10. Goense, J.B., and Logothetis, N.K. (2008). Neurophysiology of the BOLD fMRI signal in awake monkeys. Curr. Biol. *6*, 631–640.
11. Collingridge, G.L., Kehl, S.J., and McLennan, H.J. (1983). Excitatory amino acids in synaptic transmission in the Schaffer collateral-commissural pathway of the rat hippocampus. J. Physiol. *334*, 33–46.
12. Coan, E.J., Saywood, W., and Collingridge, G.L. (1987). MK-801 blocks NMDA receptor-mediated synaptic transmission and long term potentiation in rat hippocampal slices. Neurosci. Lett. *80*, 111–114.
13. Bramham, C.R., Southard, T., Sarvey, J.M., Herkenham, M., and Brady, L.S. (1996). Unilateral LTP triggers bilateral increases in hippocampal neurotrophin and trk receptor mRNA expression in behaving rats: Evidence for interhemispheric communication. J. Comp. Neurol. *368*, 371–372.
14. Amaral, D., and Lavenex, P. (2007). Hippocampal neuroanatomy. In The Hippocampus Book, P. Andersen, R. Morris, D. Amaral, T. Bliss, and J. O'Keefe, eds. (Oxford: Oxford University Press), pp. 37–114.
15. Do, V.H., Martinez, C.O., Martinez, J.L., Jr., and Derrick, B.E. (2002). Long-term potentiation in direct perforant path projections to the hippocampal CA3 region in vivo. J. Neurophysiol. *87*, 669–678.
16. Colbert, C.M., and Levy, W.B. (1993). Long-term potentiation of perforant path synapses in hippocampal CA1 in vitro. Brain Res. *606*, 87–91.

17. Yeckel, M.F., and Berger, T.W. (1990). Feedforward excitation of the hippocampus by afferents from the entorhinal cortex: Redefinition of the role of the trisynaptic pathway. Proc. Natl. Acad. Sci. USA *87*, 5832–5836.
18. Treves, A., and Rolls, E.T. (1994). Computational analysis of the role of the hippocampus in memory. Hippocampus *4*, 374–391.
19. Nakazawa, K., Quirk, M.C., Chitwood, R.A., Watanabe, M., Yeckel, M.F., Sun, L.D., Kato, A., Carr, C.A., Johnston, D., Wilson, M.A., and Tonegawa, S. (2002). Requirement for hippocampal CA3 NMDA receptors in associative memory recall. Science *297*, 211–218.
20. Stäubli, U., Thibault, O., DiLorenzo, M., and Lynch, G. (1989). Antagonism of NMDA receptors impairs acquisition but not retention of olfactory memory. Behav. Neurosci. *103*, 54–60.
21. Stäubli, U., Ivy, G., and Lynch, G. (1984). Hippocampal denervation causes rapid forgetting of olfactory information in rats. Proc. Natl. Acad. Sci. USA *81*, 5885–5887.
22. Eichembaum, H., and Cohen, N.J. (2001). From Conditioning to Conscious Recollection: Memory Systems of the Brain (New York: Oxford University Press).
23. Fuster, J.M. (2001). The prefrontal cortex–an update: Time is of the essence. Neuron *30*, 319–333.
24. Morris, R.G., Moser, E.I., Riedel, G., Martin, S.J., Sandin, J., Day, M., and O'Carroll, C. (2003). Elements of a neurobiological theory of the hippocampus: The role of activity-dependent synaptic plasticity in memory. Philos. Trans. R. Soc. Lond. B Biol. Sci. *358*, 773–786.
25. Canals, S., Makarova, I., López-Aguado, L., Largo, C., Ibarz, J.M., and Herreras, O. (2005). Longitudinal depolarization gradients along the somatodendritic axis of CA1 pyramidal cells: A novel feature of spreading depression. J. Neurophysiol. *94*, 943–951.
26. Canals, S., Lopez-Aguado, L., and Herreras, O. (2005). Synaptically recruited apical currents are required to initiate axonal and apical spikes in hippocampal pyramidal cells: Modulation by inhibition. J. Neurophysiol. *93*, 909–918.
27. Paxinos, G., and Watson, C. (2007). The Rat Brain in Stereotaxic Coordinates (New York: Academic Press, Elsevier).
28. Andersen, P., Holmqvist, B., and Voorhoeve, P.E. (1966). Entorhinal activation of dentate granule cells. Acta Physiol. Scand. *66*, 448–460.
29. Davis, S., Vanhoutte, P., Pages, C., Caboche, J., and Laroche, S. (2000). The MAPK/ERK cascade targets both Elk-1 and cAMP response element-binding protein to control long-term potentiation-dependent gene expression in the dentate gyrus in vivo. J. Neurosci. *20*, 4563–4572.
30. Oeltermann, A., Augath, M.A., and Logothetis, N.K. (2007). Simultaneous recording of neuronal signals and functional NMR imaging. Magn. Reson. Imaging *25*, 760–774.